

Original Article

A Hybrid Compressive Sensing Network for ROI-based Medical Image Recovery

A N Shilpa¹, C S Veena²

^{1,2}Department of ECE, Sambhram Institute of Technology, VTU-RC, Karnataka, India.

¹Department of ECE, Govt. Polytechnic, Channasandra, Karnataka, India.

² Department of ECE, Presidency University, Karnataka, India.

¹Corresponding Author : shilpa.an@gmail.com

Received: 11 January 2023

Revised: 27 February 2023

Accepted: 11 March 2023

Published: 29 March 2023

Abstract - The analog signals are changed to digital signals for an instance of time designed as a powerful imaging system. The imaging system produced in the digital form as it evolves the analog imaging devices has the ability to perform digital technology. Therefore, the image expansion is guided by the diagnostic system and surgical systems. The present research work used a hybrid compressive sensing algorithm consisting of an optimized neural network and lossy-lossless compression using Adaptively learned sparsifying based on L1 minimization. The Region of Interest (ROI) is compressed using Integer-based Lifting Wavelet Transform with lossless compression, and the non-ROI using an Optimized neural network. The lossy models are irreversible and achieve a higher compression ratio; therefore, the medical image processing has the visual quality in reconstruction showing compression ratio at the highest. The proposed method overcomes the dimensional reduction problem for optimizing with sparsity to non-ROI regions. Therefore, the medical image is transmitted over the network with limited bandwidth. The proposed work outcomes showed that the developed model attained a PSNR of 35.62 dB and SSIM of 0.984 better when compared to the existing ROI-CS Net model, which obtained a PSNR of 29.55 dB and SSIM of 0.89.

Keywords - Hybrid compressive sensing, Lifting wavelet transform, Optimized neural network, Region of interest.

1. Introduction

The high-resolution anatomical images generate the radiation, which has the modality performed through Magnetic resonance imaging (MRI). The MRIs have little radiation, potentially limiting the acquisition speed [1]. There are distinct acceleration models that have a fast pulse sequence which is designed as a parallel imaging model [2]. The models are applied based on the compressed sensing theory, which has attracted a wide range of research. The signals are accurately recovered based on a few measurements that represent sparsely [3]. Various compression sensing methods are employed in distinct industries, and fast MRI is evolved [4]. The k-space imaging models are accelerated significantly under-sampled, and the data fidelity and regularization process are achieved [23].

The problem of optimization is sought to minimize the regularization loss and data fidelity loss [6]. Recently, deep Convolution Neural Networks (CNN) models have been used to overcome the optimization problem [7]. The wavelet sparsity and total variation are commonly fixed based on regularizing the variants from the wavelets based on the dictionary learning models [8]. Various deep neural networks have been applied for the under-sampled MRI Reconstruction

that achieved state-of-the-art performances in terms of quality and efficiency [9].

The existing approaches were unsatisfied with medical image transmission as they showed an emerging signal processing for storage applied primarily for some measurements reduction. It reconstructed the image using a linear acquisition system and analyzed the solutions using linear schemes. The developed model has introduced lossy and lossless compression, which showed a better compression rate in terms of visual perception for image reconstruction [24].

The traditional lossless algorithms were used and applied for the ROI portion of an image. Compressive Sensing (CS) methods compress the remaining image part. The proposed method overcomes the dimensional reduction problem that optimizes using non-ROI and sparsity regions. Therefore, medical imaging techniques over the bandwidth network are limited. The contributions of the research work are as follows:

- The proposed method overcomes the dimensional reduction problems that occurred in the existing model problems.
- To optimize non-ROI and sparsity regions using BraTS and



T2-FLAIR datasets. Therefore, medical imaging techniques over the bandwidth network are limited.

The organization of the research work is given as follows: Section 2 presents the literature review, and Section 3 describes the proposed methodology. Section 4 explains the results and discussion. The conclusion of this research work is given in Section 5.

2. Literature Review

Indrarini DyahIrawati [11] developed a Lifting Wavelet Transform for performing Compressive Sensing to MRI reconstruction. The developed model used the lifting wavelet transform using the sparsity technique by considering wavelet coefficients for low pass sub-band contained important information. The developed model was useful for data compression with the highest compression ratio from the sender but remained with a higher level of accuracy. The wavelet coefficient values were arranged from the sparse vector. The research showed an effect which has arranged a sparse vector. However, the research quality must be effective to obtain better MRI quality. Further, the research did not validate the compression ratio, computational time, space-saving, and system complexity, which lowered the system's efficiency.

Xu [12] developed a Region-based Block Compressive Sensing (RBCS) with Stage Orthogonal Matching Pursuit (StOMP) algorithm. The results showed that the performances for the reconstructed components are improved than that of Block Compressive Sensing (BCS) as well as Single Spectral Compressive Sensing (SSCS) with distinct sampled ratios. However, improving the compressive sensing performances reconstructed the plant hyperspectral images based on the spatial-spectral correlation[5,10].

Zheng [13] developed a Particle Filter based Fisher Information Matrix that saved much energy and showed lesser performance. The developed model saved energy with lesser performances when compared with the optimal scenarios showed sensor observations. These observations were transmitted to the fusion center through parallel channels. The transmission number was increased with respect to the fusion center and showed super positions during observations fairly. However, the fusion center extracted the most informative data and resided the nodes for distribution.

Park [14] performed Filtered-Back Projection Region-Of-Interest Digital Tomo Synthesis (ROI-DTS). The developed model used FBP based algorithm that preserved the edge sharpening, image homogeneity, and in-plane resolution. The Compressed Sensing generates the image characteristics using

ROI-DTS was significantly different from that of the full FOV DTS. However, the model required improvement in the DTS systems.

Kawai [15] developed a Compressed SENSE-enhanced T1 high-resolution isotropic volume excitation (CS-eTHRIVE) model. The CS-eTHRIVE effectively reduced the acquisition time, which had motion artifacts that improved the image quality by using gadoteric acid. It showed enhancement based on dynamic Magnetic Resonance Imaging. However, the CS-eTHRIVE showed a sequence yielded better potentiality for focal hepatic lesion because artifacts of low motion were not used in the developed method.

LiyanSuna [16] developed a DCNN model to reconstruct undersampled MRIs. The developed model obtained ROI masks that were fed for the Reconstruction Network (RecNet) that pre-trained the MRI segmentation model (ROINET). The developed model consisted of fine-tuned RecNet, which consisted of 12 functions based on the produced ROI. However, the developed model wanted improvement in terms of quality for ROI reconstruction.

Balamurali Murugesan [17] developed a deep cascade ensemble for dual-domain networks having T1 based gradient model for perceptual refinement for MRI reconstruction. The developed Reconsynergynet (RSN) model combined the benefits of the image data independently that operates on both transforms. The multi-coil acquisition was developed and showed a variable splitting (VS-RSN) based on deep Cascade blocks. The RSN block with multi-coil DF units faithfully contains the reconstructed pathologies. The network design has various fusion feature operations that are improved through the process of attention mechanism.

Ines Njeh et al. [18] developed a deep convolutional Encoder decoder model to reconstruct brain MRI. The model fills needs among the non-learning algorithms based on the information from where any image is used for huge training information. Also, the work's main importance was to test the model with the previous dataset further.

WanyuBian et al. [19] developed an optimization technique which is based on Meta-Learning representation to reconstruct MRI with various datasets. The parameters that were regularized in the framework improved the healthiness of training and simplification of the network significantly. The major issue was that the normalization problem had occurred that needed to optimize the greater count of phases. The learning technique contained a number of stages that required more computation as it was costlier with respect to time and memory.

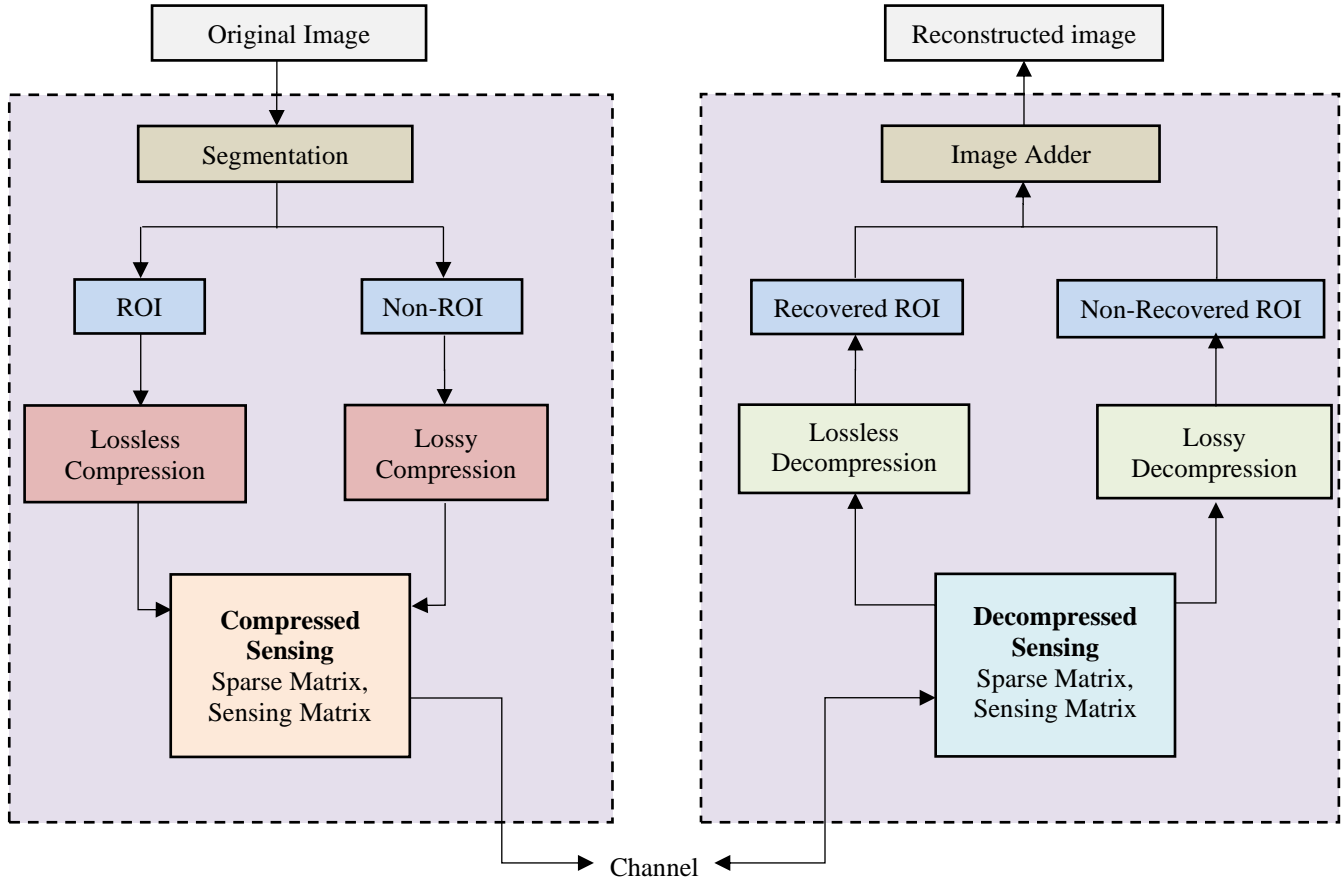


Fig. 1 An overview of the proposed methodology

3. Proposed Methodology

An overview of the proposed Hybrid Compressive Sensing model is shown in Figure 1. The proposed method steps are as follows,

3.1. Data Collection

The present research work participates in a challenge registered on the website. The training and registration data are downloaded once after collecting the data. The data consists of MR Images of 7 sets of T1 inversion recovery, and T2-FLAIR performs manual segmentations to the brain structures. Various experts performed manual segmentations for brain segmentation.

The MICCAI 2018 Grand Challenge dataset (BraTs 2018) (<https://www.med.upenn.edu/sbia/BraTs2018.html>) was used to train and evaluate the suggested architecture. Here, some data was randomly chosen, and some images were used as testing data to assess the proposed framework with existing approaches declared in the result section. Figure 2(a) is the input image, and Figure 2(b) is the threshold image.

The challenge of MRBrain S13 is that the test and training data are included a large number of pathologies. The participants are trained with their model as they are available

and submit the method to an organizer for evaluation. The test data was not released as it has 23 brain MRIs to perform manual segmentation. The collected images are publicly available, and totally of 335 images are from the BraTS 2018 dataset [21]. Among the total number of images, 76 images are from Low-Grade Glioma (LGG), and the leftover 259 images are from High-Grade Glioma (HGG) type of images. The MRI scans are focusing mainly on 3 major tasks like segmentation, intrinsic heterogeneous image based on shape and appearance, and histology images for the patient survival prediction.

3.2. Segmentation

The images are converted to grayscale images. The prospective study considers both non-ROI and ROI parts for the given image. The present research paper has emphasized the ROI part and was applied for lossless compression techniques using Huffman encoder, Arithmetic coding, and Integer Wavelet Transform. Among these encoding techniques, a suitable technique is utilized for the proposed method. The present research study emphasized the non-ROI part and was applied for the lossy compression process. The unique pixel information is retained for the stage by allowing the conventional encoding mechanism for Neural Network.

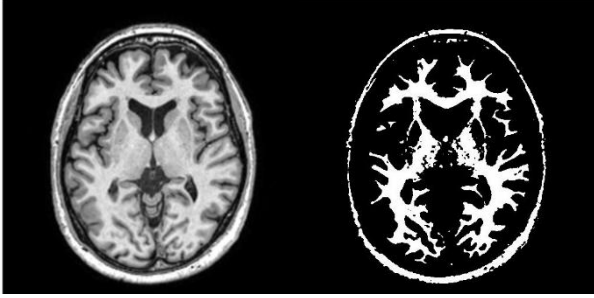


Fig. 2(a) MRBrain S13 (b) Threshold image

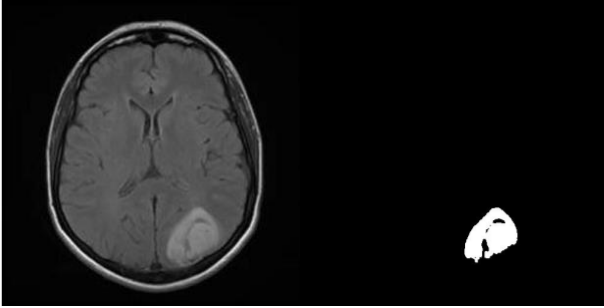


Fig. 3(a) BraTS 2018 dataset (b) Threshold image

The main advantage of compressive sensing is that data compression is reduced on the encoder side as it has less complexity. The present research work achieved real-time image compression that is done without creating computation complexity. The ROI compression and decompression are performed using lifting wavelet transform and non-ROI compression utilising an Optimized neural network.

A scene is uniformly recovered; some regions are important because of the scene among most methods. Therefore, the Region of Interest (ROI) was recovered precisely, and thus the ROI segmentation of the significant regions using the thresholding technique.

The remaining portion is accurately removed as it is the required part. Thus, the multi-level Otsu thresholding model performed the pixel separation using input images from distinct classes to perform such a function. The model then separates the levels of gray scales based on the values of intensities. Thus, the multi-Otsu thresholding finds the number of classes that are of the desired number. The main objective is to utilize Multilevel Otsu thresholding and Morphological operator technique to eliminate unwanted regions for masking based on the morphological operations. The process of morphological operations is performed based on shapes and sizes. The weights within the probabilities of the classes are evaluated based on Eq. (1).

$$q_1(t) = \sum_{i=1}^t p(i)$$

$$q_2(t) = \sum_{i=t+1}^l p(i)$$

$$q_n(t) = \sum_{i=l+t+1}^n P(i) \quad (1)$$

The threshold value ranges from 1 to t , q_1, \dots, q_n is known as the weighted class having the P as the pixel probabilities having the background and foreground images. Eq.(2) has the class means expressed in Eq. (3).

$$\mu_1(t) = \sum_{i=1}^t \frac{ip(i)}{q_1(t)}, \mu_2(t) = \sum_{i=t+1}^l \frac{ip(i)}{q_2(t)}, \dots$$

$$\mu_n(t) = \sum_{i=l+t+1}^n \frac{ip(i)}{q_n(t)} \quad (2)$$

Where, μ_1 and μ_2 are referred to as average gray level values. An input image consists of the structural elements used for performing the operations that have received the output image without losing the properties. The morphological operations for each pixel are applied for an input image corresponding to the neighborhood pixels. The image size and shape are selected based on the neighborhood pixels to perform and construct an input image.

3.3. ROI Compression and Decompression using Lifting Wavelet Transform

The process of ROI compression and decompression calculates transforms effectively. The general model was introduced for creating and generating the wavelets. The lifting-based implementation provided another wavelet transform-based lifting scheme that matched the integer to the integer process. In the present research, the lifting step $x_{o1} = s_1(z^{-1})x_e + x_0$ is approximated $x_{o1} = [s_1(z^{-1})x_e + \frac{1}{2}] + x_0$ to reach an integer value in each lifting step. This method can provide accurate reconstructions of the lifting step using $x_0 = x_{o1} - [kx_{em} + \frac{1}{2}]$. However, an issue remains with the scaling steps applied. x_{em} cannot be perfectly recovered with $x_{em} = \left(\frac{x_L}{k+1/2}\right)$.

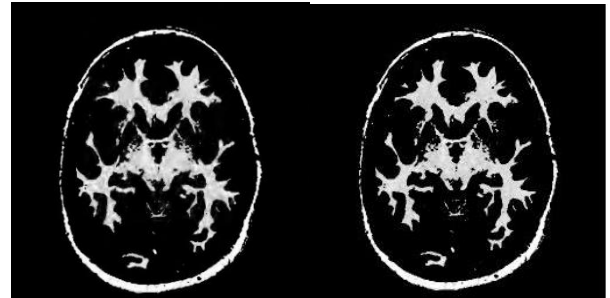


Fig. 4 ROI compression and decompression obtained for gray matter and by using the IWT model for MRBrain S13 images



Fig. 5 ROI compression and decompression obtained for gray matter and by using the IWT model for BraTS2018 images

Therefore, the approach is not lossless, and the scaling step in the wavelet transform has true values for the bi-orthogonal and orthogonal wavelet transform. The work constructed the integer-to-integer versions of several wavelets using the technique showed an integer-to-integer and classic version yield a low bit rates quality. The research utilized the integer-based wavelet transform that used the distortion of fewer data embedded and showed higher visual quality. The ROI region compression is needed because it has lower complexity and good energy compaction, which helps retain better image quality. Various integer wavelet transforms presented and utilized with zero-tree coding based on the three dimensional compression performed reconstruction for a few wavelets. Figure 4 and Figure 5 show the ROI compression and decompression obtained for gray matter using the IWT model on MRBrain S13 images and BraTS2018 images, respectively.

3.4. Non-ROI Compression and Decompression using Optimized Neural Network

Non-ROI region compression is required after performing ROI region compression and decompression. The importance of non-ROI compression is that more bits are assigned with less compression. This is capable of fewer bits, and regions are more capable of compression. The regions in an image are stable, and quality is assured. The image compression method is an application-oriented method that specifically optimizes the needed bit allocation. The proposed technique is used to optimize the neural network for the non-ROI part of an image for medical analysis. A compression of PSO and Gravitational Search Algorithm (GSA) are integrated and are modified together in terms of learning rate and the RNN weight. The RNN performed an effective compression using RNN that evaluates the MSE values. The Back Propagation performed training the RNN model that initialized the random value in terms of network parameters. There is a major limitation of the RNN model that performs compression during local optima. Thus, the GSA with PSO optimization is robustly used for global optimization based on RNN.

Firstly, the bias and weights of the RNN model are randomly selected, where the values of the MSE are executed and reach the maximum. The bias and weights are denoted with GSA agents. The fitness function for all the GSA agents is calculated at every generation, which is replaced with the worst and best agents. The GSA generates the best solution for the PSO particles. The GSA and PSO algorithms process until the values executed in a maximum number of iterations reaches the maximum. The operation phase is further performed for both compression and decompression processes until the best solution is obtained. The value of fitness is to process the optimization function, which is provided in Eq. (3).

$$k = \sum_{i=1}^m \left(\prod_{j=8(i-1)+1}^{8i} z_j \right) \quad (3)$$

Where the fitness function is represented ask m is the function dimension, z_j which is known as the values which are initialized based on the min and max image values of the pixels, the brain image reconstruction has been done through reversing process based on IDWT and RNN compression techniques. The portions of the ROI and Non-ROI were compressed individually and significantly preserved the portions of the image. The portions of the tumor images of the brain were extracted using the Otsu thresholding approach, which applied a grey histogram of an image.

The speed was high when the Otsu thresholding process occurred through the segmentation process. The compression is performed using DWT for the ROI part of an image, and the RNN model modifies the RNN attributes to learn the weights. This minimizes the losses occurring in the process of lossy compression. The proposed research objective is to achieve a better compression ratio over other brain images regarding PSNR. The RNN attributes are modified to obtain the compression of better values with fewer MSE values. Figure 6 is the non-ROI compression and decompression obtained for white matter using an optimized neural network. Figure 7 is the non-ROI compression and decompression obtained for white matter using an optimized neural network for BraTS images.

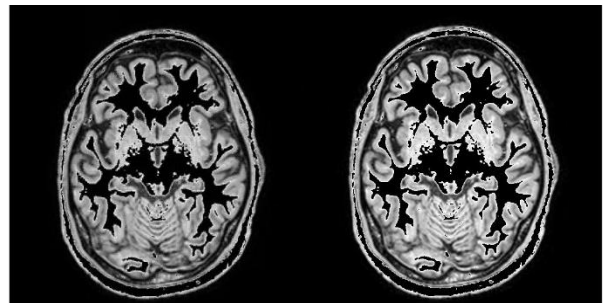


Fig. 6 Non-ROI compression and decompression obtained for white matter using optimized neural network for MRBrain S13 images

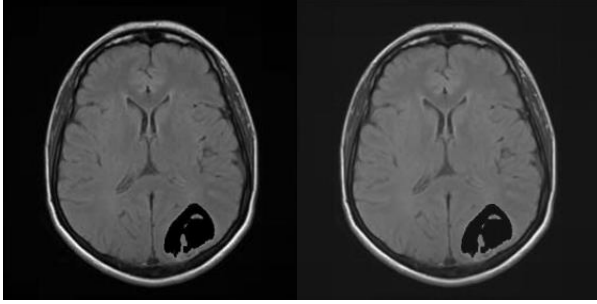


Fig. 7 Non-ROI compression and decompression obtained for white matter using optimized neural network for BraTS images

3.5. Lossless Compression and Lossy Compression using Adaptively Learned Sparsifying basis via L1 Minimization

The dictionary choice is lied for sparse key representation or is based on the sparsifying. Also, learning redundant data based on sparsifying in the best domain for the given image is important for seeking the best domain for the given image. Much effort was devoted to learning the sparsified data based on the training, where the set of training image patches, such as S are represented as $S = [s_1, s_2, \dots, s_J]$ is evaluated. There are training image patches which are having the goal to sparsify based on learning. The goal of sparsifying is by jointly learning and optimizing based on sparsifying D and represented the coefficients matrix $\Lambda = [\alpha_1, \alpha_2, \dots, \alpha_J]$ such that $s_k = D\alpha_k$ and $\|\alpha_k\|_p \leq L$. The set of training image patches is represented. The goal is to sparsifying based on learning and optimizing jointly based on D . The coefficients are represented as 1 2, ..., J such that $s_k = D\alpha_k$ and $\|\alpha_k\|_p \leq L$, where p is 0 or 1. The minimization problems are formulated as given in Eq. (4).

$$(\hat{D}, \hat{\Lambda}) = \arg \min_{D, \Lambda} \sum_{k=1}^J \|s_k - D\alpha_k\|_2^2 \text{ s.t. } \|\alpha_k\|_p \leq L, \forall k \quad (4)$$

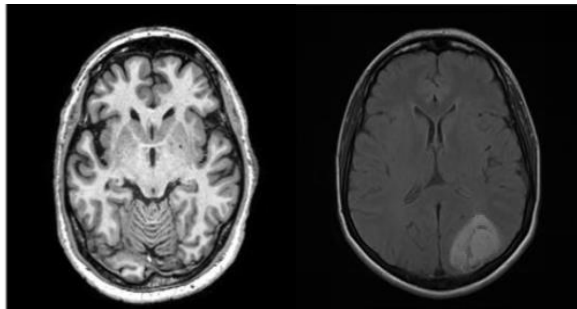


Fig. 8 Reconstructed image (a) MRBrain S13 (b) BraTS2018

The above mentioned minimization problem is mentioned in the above equation (5) and has a high convex and large scale even with $p=1$.

This is approximate, solvable and includes MOD, where the model has been proposed to optimize the values D , which led to various states of art results. Thus, to achieve an adaptive sparsifying approach, the image patches are used for training that has come from the original image. From equation 4, the original image 'x' is unavailable and has access to CS measurements, shown in equation (4). An iterative manner solves this problem for estimating alternately. [22] The medical image reconstruction is performed using the following methods.

Initially, the bit error loss is checked for receiving a signal and to compare it with the optimized reconstruction model performances. The bit error loss has occurred that performed regrouping the measurement matrix method. If it would not perform the compression for ROI and Non-ROI parts, then the Inverse transform function schemes are applied. The inverse transform function schemes are applied for the parts of ROI to process for decompression. Thus, the decompressed image for the non-ROI part is received at the output. The image obtained is added at the adder, and the original medical image is received Figure 8 shows the reconstructed image for the MRBrain S13 and BraTS2018 images.

Algorithm 1: Segmentation using a Morphological operation with OTSU's thresholding for segmenting the ROI and NON-ROI part for compression techniques and applied to compressed sensing.

- ```
//Input: The input MRI images
//Output: The reconstructed MRI images (PSNR, SSIM, NCC)
1. Load input images
2. Segmenting ROI and non-ROI parts by using morphological operation
3. Load ROI part for LWT compression.
4. Get a compressed ROI image.
5. Load NON-ROI part for optimized neural network compression.
6. Get a compressed non-ROI image.
7. Use compressed sensing technique for both compressed ROI and non-ROI parts
8. Use the reconstruction technique to reconstruct the ROI and non-ROI parts.
9. Use the Inverse LWT for decompressing the ROI part
10. Use the optimized neural network to decompress the non-ROI part
11. Get the reconstructed ROI and non-ROI part
12. To combine ROI and non-ROI to reconstruct the original image.
13. Tabulate the results.
14. Display the results.
```

Pseudo Code

Randomly generate search space of size  $N = P, (x_1^t, x_2^t, \dots, x_N^t)$  on  $P = Particle\_initialization()$ ;

For  $i=1$  to maximum iterations  
 For each particle  $p$   
 If  $p$  it is better than  $(P_{best})$   
 Calculate the fitness function using Eq. (3)  
 Evaluate fitness value  
 End for  
 End for

#### 4. Results and Discussion

The performances of the proposed Hybrid Compressive Sensing Network method, which was analysed, are shown in the present section. The proposed method is implemented onto the medical images for performing the compression by using MATLAB R2018a tool.

##### 4.1. Lossless Performance Metrics

The results for the proposed method are evaluated in terms of the following Equation (5), (6) & (7).

$$PSNR = 10 \log_{10} \left( \frac{255^2}{MSE} \right) \quad (5)$$

$$MSE = \frac{1}{pq} \sum_{x=0}^{p-1} \sum_{y=0}^{q-1} [l(x, y) - k(x, y)]^2 \quad (6)$$

$$SSIM(x, y) = \frac{(2\mu_x\mu_y + c_1)(2\sigma_{xy} + c_2)}{(\mu_x^2 + \mu_y^2 + c_1)(\sigma_x^2 + \sigma_y^2 + c_2)} \quad (7)$$

##### 4.1.1. Normalized Correlation Coefficient (NCC)

The average difference is the sum of the differences among the consecutive number pairs, which obtains the average value divided by the total number of pairs.

The Normalized Correlation Coefficient is expressed as shown in Eq. (8).

$$norm_{corr}(x, y) = \frac{\sum_{n=0}^{n-1} x[n] * y[n]}{\sqrt{\sum_{n=0}^{n-1} x[n]^2 * \sum_{n=0}^{n-1} y[n]^2}} \quad (8)$$

##### 4.1.2. Normalized Average Error (NAE)

NAE is a statistical calculation used for comparing proficiency and testing the results where the measurement of results is uncertain.

Where ' $p$ ' and ' $q$ ' are taken as row and column of the image,  $k(x, y)$  is taken as decrypted images, and  $l(x, y)$  is taken as the original input image.

Where, ' $x$ ' and ' $y$ ' are defined as windows of filter image ' $k$ ' and original image ' $I$ ', ' $\sigma$ ' and ' $\mu$ ' are denoted as standard deviation and mean of ' $x$ ' and ' $y$ ', ' $c_1$ ' and ' $c_2$ ' are indicated as constants.

##### 4.2. Quantitative Analysis

Table 1 gives obtained results from the proposed work evaluated terms of MSE, PSNR, AD, SSIM, NAE, and NCC for an image's ROI and non-ROI parts. The ROI part and non-ROI regions in an image are reconstructed and obtain PSNR of 33.81, MSE of 0.022, NCC of 0.982, AD of 0.409, SSIM of 0.988, and NAE of 0.181.

Figure 9 shows the Comparison of ROI and Non-ROI parts of an image. Table 2 gives the results achieved for the proposed method in terms of PSNR, MSE, NCC, AD, SSIM, and NAE evaluated for the gray matter and White matter.

From Table 2, The Gray matter and White matter in an image are reconstructed and obtain PSNR of 35.82, MSE of 0.027, NCC of 0.979, AD of 0.385, SSIM of 0.980, and NAE of 0.177. Figure 10 shows a Comparison of the Gray matter and white matter part of an image.

Table 3 obtains the proposed method results evaluated in terms of PSNR, MSE, NCC, AD, SSIM, and NAE with respect to the Splenium for the corpus callosum and the non-ROI part for an image.

The part of Splenium of the corpus callosum and non-ROI part of an image is reconstructed and obtains PSNR of 37.22, MSE of 0.054, NCC of 0.974, AD of 0.411, SSIM of 0.982, and NAE of 0.154. The present research work obtains overall compression reconstruction for compressed sensing. Elapsed time is 960.95 seconds.

**Table 1. Results achieved for the proposed technique in terms of PSNR, MSE, NCC, AD, SSIM, and NAE for ROI, non-ROI part**

| Image               | PSNR   | MSE   | NCC   | AD    | SSIM  | NAE   |
|---------------------|--------|-------|-------|-------|-------|-------|
| ROI part            | 28.371 | 0.068 | 0.977 | 0.775 | 0.971 | 0.105 |
| Non-ROI part        | 29.87  | 0.024 | 0.983 | 0.077 | 0.920 | 0.153 |
| Reconstructed Image | 33.815 | 0.022 | 0.982 | 0.409 | 0.988 | 0.181 |

**Table 2. Results achieved for the proposed technique in terms of PSNR, MSE, NCC, AD, SSIM, and NAE for gray and white matter**

| Images        | PSNR  | MSE   | NCC   | AD    | SSIM  | NAE   |
|---------------|-------|-------|-------|-------|-------|-------|
| Gray matter   | 32.52 | 0.053 | 0.979 | 0.808 | 0.968 | 0.108 |
| White matter  | 33.66 | 0.023 | 0.981 | 0.143 | 0.924 | 0.162 |
| Reconstructed | 35.82 | 0.027 | 0.979 | 0.385 | 0.980 | 0.177 |

**Table 3. Results achieved for the proposed technique in terms of PSNR, MSE, NCC, AD, SSIM, and NAE for Splenium of corpus callosum part for non-ROI and reconstructed part in an image**

| Regions       | PSNR  | MSE   | NCC   | AD    | SSIM  | NAE   |
|---------------|-------|-------|-------|-------|-------|-------|
| Non-ROI part  | 38.89 | 0.090 | 0.962 | 0.170 | 0.914 | 0.135 |
| Reconstructed | 37.22 | 0.054 | 0.974 | 0.411 | 0.982 | 0.154 |

**Table 4. Results achieved for the proposed technique in terms of PSNR, MSE, NCC, AD, SSIM, and NAE for the BraTS dataset**

| Regions       | PSNR  | MSE   | NCC   | AD     | SSIM  | NAE   |
|---------------|-------|-------|-------|--------|-------|-------|
| ROI (Tumor)   | 52.99 | 0.003 | 0.993 | 0.0092 | 0.999 | 0.036 |
| Non-ROI part  | 46.01 | 0.016 | 0.991 | 0.011  | 0.989 | 0.026 |
| Reconstructed | 41.68 | 0.044 | 0.996 | 0.0115 | 0.975 | 0.033 |

**Table 5. Compressive sensing ratio**

| CS Ratio | PSNR  | MSE    | NCC   | AD    | SSIM  | NAE   |
|----------|-------|--------|-------|-------|-------|-------|
| 10%      | 39.3  | 0.0011 | 0.993 | 0.117 | 0.963 | 0.052 |
| 20%      | 40.89 | 0.0012 | 0.99  | 0.072 | 0.97  | 0.043 |
| 30%      | 42.4  | 0.0044 | 0.995 | 0.035 | 0.978 | 0.025 |
| 40%      | 42.03 | 0.004  | 0.992 | 0.073 | 0.977 | 0.035 |

**Table 6. Comparative analysis**

| Method                                            | Dataset     | PSNR  | SSIM   |
|---------------------------------------------------|-------------|-------|--------|
| Lifting Wavelet Transform [11]                    | MRBrain S13 | -     | 0.7551 |
| Reconstruction Network (RecNet) [16]              |             | 31.82 | 0.894  |
| Ensemble of dual-domain networks [17]             |             | -     | 0.878  |
| Deep Convolutional Encoder-Decoder algorithm [18] | BraTS2018   | 39.58 | 0.9618 |
| Proposed Hybrid Compressive method                | MRBrain S13 | 35.62 | 0.984  |
|                                                   | BraTS2018   | 41.68 | 0.977  |

**Table 7. Compressive sensing ratio compared among proposed and existing models with respect to the MRBrain S13 dataset**

| CS ratio | Methods            | PSNR    | SSIM   |
|----------|--------------------|---------|--------|
| 10%      | Proposed Hybrid CS | 39.3    | 0.963  |
|          | Meta-learning [19] | 22.043  | 0.6279 |
| 20%      | Proposed Hybrid CS | 40.89   | 0.97   |
|          | Meta-learning [19] | 24.7162 | 0.697  |
| 30%      | Proposed Hybrid CS | 42.4    | 0.978  |
|          | Meta-learning [19] | 26.45   | 0.735  |
| 40%      | Proposed Hybrid CS | 42.03   | 0.977  |
|          | Meta-learning [19] | 27.53   | 0.77   |

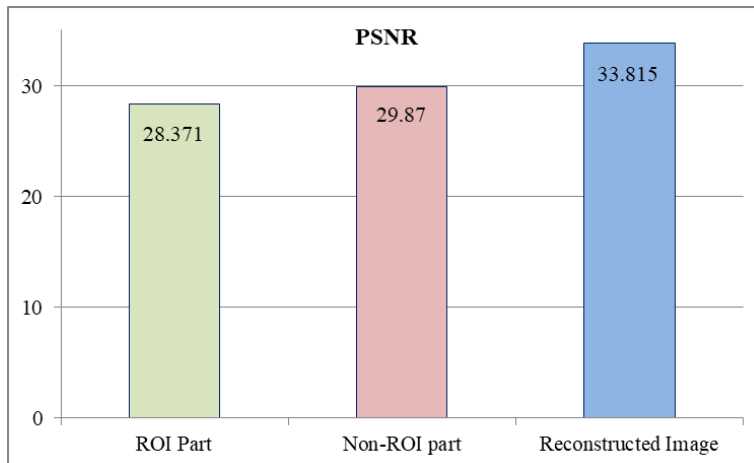


**Fig. 9 Comparison of ROI and Non-ROI parts of an image**

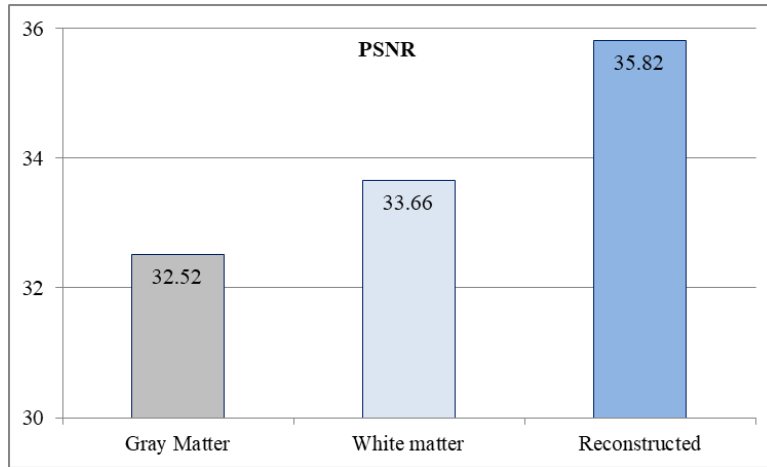


Fig. 10 Comparison of gray matter and white matter part of an image

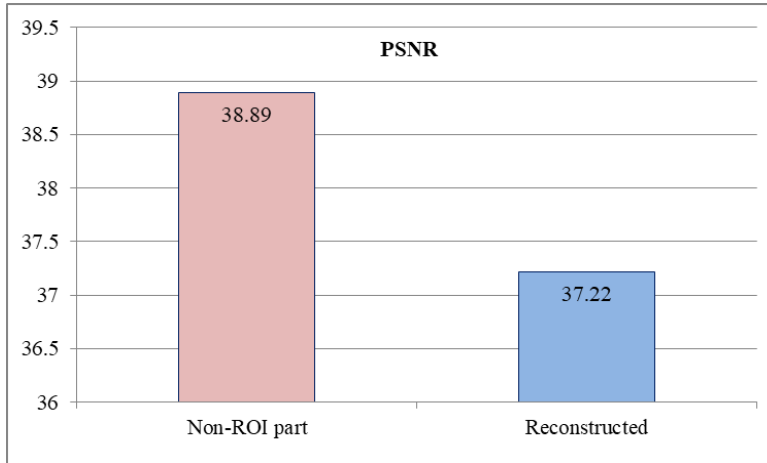


Fig. 11 PSNR values to the Splenium of the corpus callosum with the Non-ROI and reconstructed part

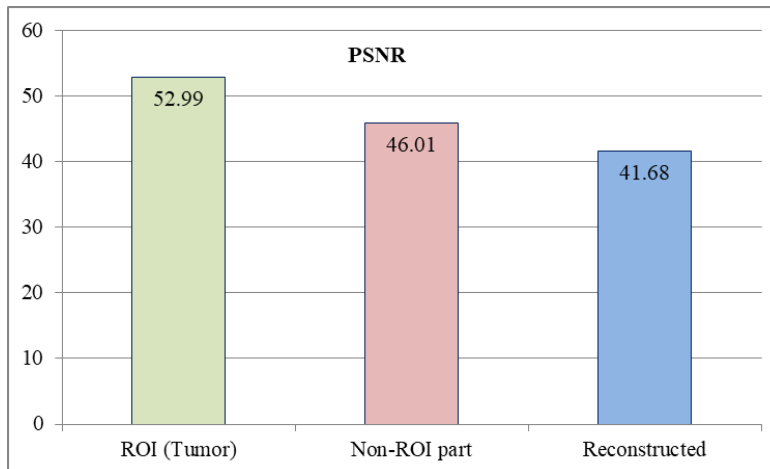


Fig. 12 PSNR values of ROI, Non-ROI and reconstructed part for BraTS dataset

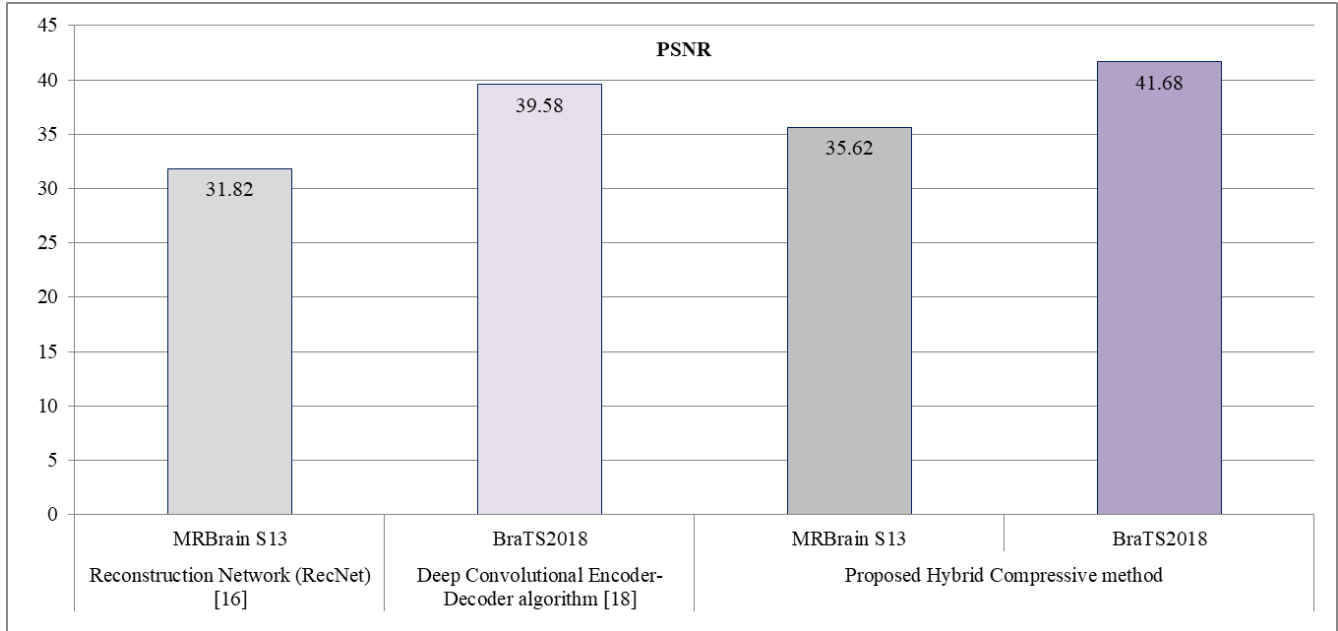


Fig. 13 PSNR values in comparative analysis

Figure 11 shows the PSNR values to the Splenium of the corpus callosum with the Non-ROI and reconstructed part. The Compressed sensing obtained an Elapsed time of 87.96 seconds. Similarly, over (Reconstruction) compressed sensing Elapsed time is 1474.3 seconds and Compressed sensing Elapsed time is 317.7 seconds.

Table 4 displays the results achieved for the proposed method in terms of PSNR, MSE, NCC, AD, SSIM, and NAE for the BraTS dataset. Table 5 shows the Quantitative results of PSNR, MSE, NCC, AD, NAE and SSIM using a dataset with different sampling rates.

#### 4.3. Comparative Analysis

Table 6 gives a comparative analysis done among the available methods. The existing Lifting Wavelet Transform method obtained an SSIM of 0.7551. Similarly, the MRI reconstruction network obtained a PSNR of 31.82 dB and SSIM of 0.894. Whereas the proposed method obtained a PSNR of 35.62 dB and SSIM of 0.984 were better when compared to the available methods. The existing models showed a recovery quality in ROIs improvement that made the network focus on loss function, recovered the ROI and obtained 29.55 dB of PSNR.

Similarly, fine-tuning was performed for the network reconstruction that provides better quality reconstructions on the ROI obtained 31.82 dB of PSNR.

Similarly, the existing model constructed the network design where the feature fusion operations were performed to improve through attention mechanisms obtained SSIM of

0.878. The proposed Hybrid Compressive sensing showed better values of PSNR and SSIM of 35.62 and 0.984. Table 7 shows Compressive Sensing Ratio compared among the proposed and the existing Meta-learning model with respect to the MRI dataset.

## 5. Conclusion

The present research work used a hybrid Compressive Sensing Algorithm from where the Region of Interest is compressed with lossless compression and the non-ROI. The lossy models are irreversible and achieve higher compression ratio visual quality during image reconstruction showed better Compression Ratio. The existing approaches were not satisfied with medical image transmission as they showed an emerging signal processing for storage. Initially, the bit error loss is checked for receiving a signal and to compare it with the optimized reconstruction model performances. The bit error loss has occurred that performed regrouping the measurement matrix method. If it does not perform the compression for ROI and Non-ROI parts, then the Inverse transform function schemes are applied. The inverse transform function schemes are applied for the parts of ROI to process for decompression.

Thus, the decompressed image for the non-ROI part is received at the output. The proposed method results showed that the model attained a PSNR of 35.62 dB and SSIM of 0.984 better when compared to the existing ROI-CSNet-based model obtained a PSNR of 29.55 dB and SSIM of 0.89. However, in the future, an image's ROI and non-ROI parts can be subdivided into lossy and lossless components to improve the complexity problem more effectively.

## References

- [1] Mingli Zhang et al., ‘Robust Brain MR Image Compressive Sensing Via Re-weighted Total Variation and Sparse Regression,’ *Magnetic Resonance Imaging*, vol. 85, pp. 271–286, 2022. [[CrossRef](#)] [[Google Scholar](#)] [[Publisher Link](#)]
- [2] Morteza Mardani et al., ‘Deep Generative Adversarial Neural Networks for Compressive Sensing MRI,’ *IEEE Transactions on Medical Imaging*, vol. 38, no. 1, pp. 167–179, 2019. [[CrossRef](#)] [[Google Scholar](#)] [[Publisher Link](#)]
- [3] Minghui Zhang et al., ‘High-dimensional Embedding Network Derived Prior for Compressive Sensing MRI Reconstruction,’ *Medical Image Analysis*, vol. 64, p. 101717, 2020. [[CrossRef](#)] [[Google Scholar](#)] [[Publisher Link](#)]
- [4] Yan Yang et al., ‘ADMM-CSNet: A Deep Learning Approach for Image Compressive Sensing,’ *IEEE Transactions on Pattern Analysis and Machine Intelligence*, vol. 42, no. 3, pp. 521–538, 2020. [[CrossRef](#)] [[Google Scholar](#)] [[Publisher Link](#)]
- [5] Agouzal Mehdi, Merzouqi Maria, and Moha Arouch, ‘An Original Method of Extraction Bands Based On Spectral And Spatial Characteristic To Reduce The Hyperspectral Image,’ *International Journal of Engineering Trends and Technology*, vol. 70, no. 1, pp. 185-194, 2022. [[CrossRef](#)] [[Publisher Link](#)]
- [6] Shrividya Guruprasad, S. H. Bharathi, and D. Anto Ramesh Delvi, ‘Effective Compressed Sensing MRI Reconstruction Via Hybrid GSGWO Algorithm,’ *Journal of Visual Communication and Image Representation*, vol. 80, p. 103274, 2021. [[CrossRef](#)] [[Google Scholar](#)] [[Publisher Link](#)]
- [7] Xiaohong Fan, Yin Yang, and Jianping Zhang, ‘Deep Geometric Distillation Network for Compressive Sensing MRI,’ *2021 IEEE EMBS International Conference on Biomedical and Health Informatics (BHI)*, pp. 1–4, 2021. [[CrossRef](#)] [[Google Scholar](#)] [[Publisher Link](#)]
- [8] Guillermo Marzik, Shin-ichi Sato, and Mariano Ezequiel Girola, ‘Compressive Sensing for Perceptually Correct Reconstruction of Music and Speech Signals,’ *Applied Acoustics*, vol. 183, p. 108328, 2021. [[CrossRef](#)] [[Google Scholar](#)] [[Publisher Link](#)]
- [9] Hong Lu et al., ‘Deep Convolutional Neural Network for Compressive Sensing of Magnetic Resonance Images,’ *International Journal of Pattern Recognition and Artificial Intelligence*, vol. 35, no. 15, p. 2152019, 2021. [[CrossRef](#)] [[Google Scholar](#)] [[Publisher Link](#)]
- [10] Vidyasagar Talwar, and B.S.Sohi, ‘Dimensionality Reduction of Hyperspectral Image Using Different Methods,’ *International Journal of Engineering Trends and Technology*, vol. 69, no. 2, pp. 139-143, 2021. [[CrossRef](#)] [[Publisher Link](#)]
- [11] Indrarini Dyah Irawati et al., ‘Lifting Wavelet Transform in Compressive Sensing for MRI Reconstruction,’ *Journal of Southwest Jiaotong University*, vol. 55, no. 5, 2020. [[CrossRef](#)] [[Google Scholar](#)] [[Publisher Link](#)]
- [12] Ping Xu et al., ‘A Region-based Block Compressive Sensing Algorithm for Plant Hyperspectral Images,’ *Computers and Electronics in Agriculture*, vol. 162, pp. 699–708, 2019. [[CrossRef](#)] [[Google Scholar](#)] [[Publisher Link](#)]
- [13] Yujiao Zheng et al., ‘Compressive Sensing Based Probabilistic Sensor Management for Target Tracking in Wireless Sensor Networks,’ *IEEE Transactions on Signal Processing*, vol. 63, no. 22, pp. 6049–6060, 2015. [[CrossRef](#)] [[Google Scholar](#)] [[Publisher Link](#)]
- [14] Soyoung Park et al., ‘Image Reconstruction in Region-of-interest (or interior) Digital Tomosynthesis (DTS) Based on Compressed-Sensing (CS),’ *Computer Methods and Programs in Biomedicine*, vol. 151, pp. 151–158, 2017. [[CrossRef](#)] [[Google Scholar](#)] [[Publisher Link](#)]
- [15] Nobuyuki Kawai et al., ‘Gadoxetic Acid-enhanced Dynamic Magnetic Resonance Imaging using Optimized Integrated Combination of Compressed Sensing and Parallel Imaging Technique,’ *Magnetic Resonance Imaging*, vol. 57, pp. 111–117, 2019. [[CrossRef](#)] [[Google Scholar](#)] [[Publisher Link](#)]
- [16] Liyan Sun et al., ‘Region-of-interest Undersampled MRI Reconstruction: A Deep Convolutional Neural Network Approach,’ *Magnetic Resonance Imaging*, vol. 63, pp. 185–192, 2019. [[CrossRef](#)] [[Google Scholar](#)] [[Publisher Link](#)]
- [17] Balamurali Murugesan et al., ‘A Deep Cascade of Ensemble of Dual Domain Networks with Gradient-based T1 Assistance and Perceptual Refinement for fast MRI Reconstruction,’ *Computerized Medical Imaging and Graphics*, vol. 91, p.101942, 2021. [[CrossRef](#)] [[Google Scholar](#)] [[Publisher Link](#)]
- [18] Ines Njeh et al., ‘Deep Convolutional Encoder-Decoder Algorithm for MRI Brain Reconstruction,’ *Medical & Biological Engineering & Computing*, vol. 59, pp.85-106, 2021. [[CrossRef](#)] [[Google Scholar](#)] [[Publisher Link](#)]
- [19] Wanyu Bian et al., ‘An Optimization-Based Meta-Learning Model for MRI Reconstruction with Diverse Dataset,’ *Journal of Imaging*, vol. 7, no. 11, 2021. [[CrossRef](#)] [[Google Scholar](#)] [[Publisher Link](#)]
- [20] G. Vijayalakshmi, Sudipto Biswas, and Sankeerth Reddy, ‘Semantic Understanding of Abstract Images,’ *SSRG International Journal of Computer Science and Engineering*, vol. 4, no. 4, pp. 30-34, 2017. [[CrossRef](#)] [[Publisher Link](#)]
- [21] Adrienne M. Mendrik et al., ‘MRBrainS Challenge: Online Evaluation Framework for Brain Image Segmentation in 3T MRI Scans,’ *Computational Intelligence and Neuroscience*, 2015. [[CrossRef](#)] [[Google Scholar](#)] [[Publisher Link](#)]
- [22] P.Kanmani, P.Marikkannu, and M.Brindha, ‘A Medical Image Classification using ID3 Classifier,’ *SSRG International Journal of Computer Science and Engineering*, vol. 3, no. 10, pp. 8-11, 2016. [[CrossRef](#)] [[Google Scholar](#)] [[Publisher Link](#)]

- [23] Mohamed Ragab, Osama A. Omer, and Mohamed Abdel-Nasser, "Compressive Sensing MRI Reconstruction using Empirical Wavelet Transform and Grey Wolf Optimizer," *Neural Computing and Applications*, vol. 32, pp. 2705–2724, 2020. [[CrossRef](#)] [[Google Scholar](#)] [[Publisher Link](#)]
- [24] Ejaz Ul Haq et al., "Block-based Compressed Sensing of MR Images using Multi-rate Deep Learning Approach," *Complex & Intelligent Systems*, vol. 7, pp. 2437–2451, 2021. [[CrossRef](#)] [[Google Scholar](#)] [[Publisher Link](#)]